

THE INCUBATOR
Journal of Postgraduate Studies, FULafia

journal homepage:
https://journals.fulafia.org.ng/index.php/incubator/index

Research paper

Low-Dose X-Ray-Induced Changes in Rat Skin Dielectric Properties and Microstructure: A Cole-Cole and SEM Study

S. M. Orkaa[1,*], A. A. Bello[2], J. Z. Dlama[3], A. M. Hamza[2], and J. U. Ewuga[4]

[1] *Department of Radiography and Radiation Science, Rev. Fr. Moses Orshio Adasu University, Makurdi, Benue State, Nigeria.*
[2] *Department of Physics, Federal University of Lafia, PMB 146, Lafia, Nasarawa State, Nigeria.*
[3] *Department of Radiography and Radiation Science, Federal University of Lafia, PMB 146, Lafia, Nasarawa State, Nigeria.*
[4] *Department of Physics, Karl Kum University, Vom, Plateau State, Nigeria*

ARTICLE INFO

Received: 04/08/2026
Received in revised form: 03/10/2026
Accepted: 20/10/2026
Available online: 30/10/2026

DOI: 10.62050/incubator.2026.1.1.51

Keywords:
Dielectric spectroscopy, Cole-Cole relaxation model, Low-dose X-ray, Cutaneous tissue biophysics

ABSTRACT

In soft tissues, low-dose ionizing radiation produces subtle, subclinical radiochemical and structural changes that frequently go undetected by conventional histopathological methods. The low-frequency (20 Hz–20 kHz) dielectric shifts and microstructural abnormalities in healthy versus X-irradiated (0–5.25 mGy) albino rat skin are measured and modelled in this study. A bespoke parallel-plate sample cell was used to analyze ex vivo skin tissue at 37 °C. Cole-Cole parameters were retrieved and associated with 3D axisymmetric COMSOL Multiphysics X-ray beam propagation simulations and surface topographies from scanning electron microscopy (SEM). Core capacitive parameters underwent a monotonic collapse as a result of X-ray irradiation. A significant decrease in static permittivity (ε_s from 22.84 to 7.29) and a similar decrease in dielectric strength ($\Delta\varepsilon$) were noted at 5.25 mGy, indicating reduced polarization as a result of structural protein denaturation. At the same time, typical relaxation periods (τ) decreased from 41 to 14 μs, suggesting that macromolecules were breaking up into smaller, quickly reorienting dipolar units. A change from a loose, healthy fibre web to a compacted, fragmented matrix was verified by SEM. Peak energy deposition (~8 J/kg) was localized by COMSOL simulations close to a 3 mm focal depth. By jeopardizing membrane integrity, low-dose radiation significantly impairs skin macroscopic bioelectrical properties, facilitating the creation of non-invasive bioimpedance sensors.

© 2026 The Author(s). Published by College of Postgraduate Studies, Federal University of Lafia, Nigeria under the terms of the Creative Commons Attribution 4.0 International license. Further distribution of this work must maintain attribution to the author(s) and the published article's title, journal citation, and DOI.

INTRODUCTION

The skin, which covers the whole skin surface to provide an active regulatory barrier, is the largest and most physiologically complex organ in the mammalian body. It performs essential multifunctional roles, modulating transcutaneous electrolyte preservation and thermoregulatory homeostasis while acting as a primary physical, chemical, and biological barrier against environmental harm such as mechanical stress, thermal fluctuations, toxic substances, and solar ultraviolet radiation (Iyomasa et al., 2014). The non-viable stratum corneum, the living epidermis, the vascularized dermis, and the fatty adipose architecture of the hypodermis are the several morphological sub layers that make up the skin, which is described biophysically as a highly lossy, directed layered tissue structure (Huclova et al., 2012). The arrangements of cells and material compositions of each sub layer are extremely different, leading directly to incredibly different electrical and dielectric characteristics.

Electrical impedance spectroscopy (EIS) and broadband dielectric spectroscopy have become very sensitive analytical methods in modern biomedical engineering to non-invasively examine these different cellular

*Corresponding author email: orkaastephen@gmail.com (S. M. Orkaa).

domains. EIS has been effectively used to detect precancerous changes in cervical squamous tissue (Walker et al., 2002), detect cutaneous malignancies (Aberg et al., 2005), track localized skin irritations (Ferreira et al., 2007), assess ischemic boundaries (Marzec 2005), and measure edematous fluid shifts in damaged tissue profiles (Huclova et al., 2012). This is because the abnormalities of the body's state affect the structure of the cell and its surrounding substances. Estimating the amount of energy absorbed by the cells and their physiological condition in real-time requires accurate measurements of tissue-specific complex permittivity ($\varepsilon^* = \varepsilon' - j\varepsilon'$) over different frequency spectra (Zimmermann & Rienen, 2021). While there have been developments in this regard (Orkaa et al., 2024), the problem with continuous, ultra-low frequency (sub-1 kHz) dielectric profiling of multiple layers of skin in case of low-dose ionizing radiation remains unsolved in bioelectromagnetics literature.

Conversely, low dose regimes (milligray range) induce subtle radiochemical modifications, denaturation of structural proteins and permeabilization of cell membranes, not always detectable by conventional histopathological techniques. High dose X-ray exposure induces immediate macromolecular fragmentation and evident cell death. Ionising radiation causes a uniform decrease in boundary capacitances, a change in extracellular matrix density and a change in localised electrolyte balances (Zimmermann & Rienen, 2021). At present, there are very few systematic frameworks that combine controlled low-dose in vivo rodent irradiation, accurate regional dosimetric mapping using calibrated thermoluminescent dosimeter (TLD) phantoms, structural verification using scanning electron microscopy (SEM), and computational X-ray propagation modelling using COMSOL Multiphysics.

To overcome this biophysical limitation, the current study systematically evaluates and models the frequency-dependent dielectric changes of epidermal tissues extracted from healthy albino rats exposed to low-dose X-ray settings (0 to 5.25 mGy). A custom-made, parallel-plate Perspex sample cell is constructed following known coaxial measurement designs and real permittivity (ε') and bulk conductivity are measured over the important low-frequency to radiofrequency range (20 Hz to 20 kHz). In this work, the essential biophysical features such as static permittivity (εs), high-frequency permittivity ($\varepsilon\infty$), dielectric strength ($\Delta\varepsilon$), characteristic relaxation time (τ) and the distribution spread parameter (α) are extracted and separated by using the Cole-Cole relaxation model. These experimental profiles are essentially compared with high resolution SEM topographies and 3D Axisymmetric COMSOL energy-deposition simulations. Ultimately, our work provides a strict baseline for the detection of early-stage subclinical tissue damage, which is an immediate aid for the development of therapeutic radiation monitoring methods and non-invasive bioimpedance sensors.

MATERIALS and METHODS

An XD4-2.9/100 mobile X-ray generator was used to expose 200 g albino rats to X-ray radiation while they were in a prone position. The system was run with a total filtration of 2.9 mmAl and a voltage range of 65–95 kV at a current of 32 mA. A focus-to-skin distance (FSD) of 40 cm was maintained to ensure uniform coverage of the whole body and the radiation field size was carefully constrained by collimation. Five (5) rat samples were irradiated with specified doses of radiation measured by thermoluminescent dosimeter (TLD) chips. The TLD chips were collected after exposure, stored in air tight containers and transported for read out examination. A total of six (6) albino rats were used for this study.

After irradiation, the rats were killed by suffocation to allow immediate removal of the target tissues. Measurements of the dielectric properties of the separated skin tissue samples were immediately recorded at a controlled physiological temperature of 37 °C. The sample was stored in a sterile, airtight sealed container to keep the integrity of the sample during the measuring procedure.

A parallel plate sample cell was constructed from Perspex material following the experimental technique of Agba et al. (2008). The cell used a plastic syringe with an inner diameter of 0.947 cm to allow for an adjustable inter-electrode separation of 3.2 cm. The sample cell was connected to a measuring circuit composed of a TH 27 conductometer, a JDS66 DDS signal generator and a STEREN digital capacitance meter through clip test leads to enable real-time dielectric characterisation of the biological specimens. Such an arrangement allowed electrical conductivity and capacitance measurements to be made directly at a range of frequencies.

SEM Analysis

Following X-ray irradiation, skin tissue samples were taken from a group of albino rats. Following that, both the experimental (irradiated) and control (non-irradiated) specimens underwent ultra-structural analysis. This analysis was done by firstly, dehydrating the tissue samples to remove all moisture and prevent structural collapse. To facilitate imaging, the tissues were then thinly sectioned. All prepared samples were examined using scanning electron microscopy (SEM) to describe the structural alterations caused by radiation. The Zeiss Gemini 1-Sigma 300 equipment needed for high-resolution imaging and tissue assessment was supplied by the Nigerian Building and Road Research Institute (NBRRI) in Abuja, and it was utilized for the SEM investigation.

Model for X-ray Beam Propagation in Tissue

COMSOL Multiphysics software, version 5.5, was used to simulate the absorption of X-rays in biological tissues. Here, high energy radiation is tracked as it travels through a substance and loses energy in order to simulate X-ray absorption. Beer-Lambert law is used in this.

Using a 2D axisymmetric formulation within the COMSOL Multiphysics software environment, a computational model was built to assess the X-ray beam's spatial dispersion and depth penetration. By using angular symmetry, this geometric optimization significantly reduces computational cost while maintaining spatial precision along the main propagation axis (z-axis). A thick cylindrical phantom designed to simulate multi-layered biological domains served as a representation of the goal geometry.

In simulating a monochromatic spectrum, a parametric sweep was executed over a discrete range of photon energies, E. Energy dependent material characteristics were incorporated into the model by interpolating experimental mass attenuation coefficients (μ/ρ) across the varying incident spectrum. The incident X-ray beam intensity (I0) was discretely defined utilizing a structured indexing system assigned to the two primary biological tissue components under investigation.

Material transitions and structural boundaries within the phantom were dynamically handled via a switch expression, enabling smooth spatial segmentation. The underlying mathematical physics domain governed radiation transport and subsequent energy deposition, mapping the localized absorbed dose (D, measured in J/kg) across the geometry. Following the execution of the parametric sweep, the resulting attenuating profiles and depth-dose distributions were post-processed and visualized along the central axis of propagation.

RESULTS

Table 1

Values of Dielectric Permittivity, ε′ For X-Irradiated and Non-Irradiated (Control) Healthy Rats' Skin Tissues at Selected Frequencies

F (kHz) / Dose (mGy)	0.02	0.1	0.3	0.6	0.8	1	2	5	8	10	15	20
0 (control)	22.8	4512.3	-	724.2	537.6	426.4	203.2	71.9	39.2	28.3	13.8	8.7
0.15	19.4	3840.3	1258.9	616.3	457.5	362.9	172.9	61.2	33.3	24.1	11.7	7.4
0.67	12.2	2400.2	787.4	385.2	285.9	226.8	108.1	38.2	20.8	15.1	7.3	4.6
1.35	10.7	2112.2	692.9	338.9	251.6	199.6	95.1	33.6	18.3	13.3	6.5	4.1
2.50	9.7	1920.1	629.9	308.2	228.8	181.4	86.5	30.6	16.7	12.1	5.9	3.7
5.25	7.3	1440.1	472.5	231.1	171.6	136.1	64.9	22.9	12.5	9.0	4.4	2.8

According to accepted biophysical principles, the control group (0 mGy) in Table 1 displays typical dielectric dispersion behaviour (Gabriel et al., 1996). Significant ε' variance across frequencies (4512.315 at 0.1 kHz vs. 8.7 at 20 kHz) and a rapid ε' decay as the dose increases compatible with Maxwell-Wagner interfacial polarization effects are shown in the data (Pethig, 2018). All radiation doses exhibit notable changes in ε' when compared to the control, with a maximum and minimum effect noted at 0.1 kHz and 20 kHz, respectively, and a progressive ε' drop with increasing dose (most prominent at 5.25 mGy).

Table 2

Values for Conductivity, σ for X-Irradiated and Non-Irradiated (Control) Healthy Rats' Skin Tissues at Selected Frequencies.

F (kHz) / Dose (mGy)	0.02	0.1	0.3	0.6	0.8	1	2	5	8	10	15	20
0 (control)	6.85	7.55	-	7.0	7.0	6.9	6.75	5.8	4.40	3.65	3.70	4.35
0.15	6.8	6.9	6.8	6.75	6.8	6.85	6.70	5.7	4.35	3.60	3.55	4.35
0.67	6.55	6.95	6.9	6.85	6.9	6.85	6.65	5.75	4.40	3.60	3.60	4.30
1.35	6.95	7.60	9.05	7.05	7.05	6.95	6.70	5.80	4.45	3.65	3.70	4.30
2.50	6.8	7.05	8.45	4.95	6.95	6.95	1.15	5.75	4.40	3.60	3.60	4.25
5.25	6.80	7.10	7.10	7.05	7.0	7.0	6.65	5.85	4.5	3.65	3.55	3.40

Table 3

Dielectric Parameter Obtained from Dielectric Dispersion and Cole-Cole Plots for X-Irradiated and Non-Irradiated Rat Skin

Dose (mGy)	ε_s	ε_∞	$\Delta(\varepsilon_s - \varepsilon_\infty)$	F_R(Hz)	$\tau(\mu s)$	α
0	22.84	8.71	14.13	20	41	0.07
0.15	19.44	7.41	12.03	20	41	0.06
0.67	12.15	4.63	7.52	20	22	0.04
1.35	10.69	4.08	6.61	20	19	0.03
2.50	9.72	3.71	6.01	20	21	0.03
5.25	7.29	2.78	4.51	20	14	0.02

Table 3's data shows a notable deterioration of dielectric characteristics caused by radiation. Static permittivity εs, high frequency permittivity ε∞, and dielectric strength Δ all show a monotonic decline with increasing dose. It is noted that the εs declines from 22.84 to 7.29 indicating a loss of the polarization capability of the material. This signifies that radiation reduces the amount of dipole moments in a material (Kremer & Schönhals, 2003).

Also, the relaxation time decreases from 41 μs to 14 μs non-linearly. This shows that as a result of radiation damage, the rest of the polarization process moves fast thereby reducing the energy barriers for charge migration (Jonscher, 1999).

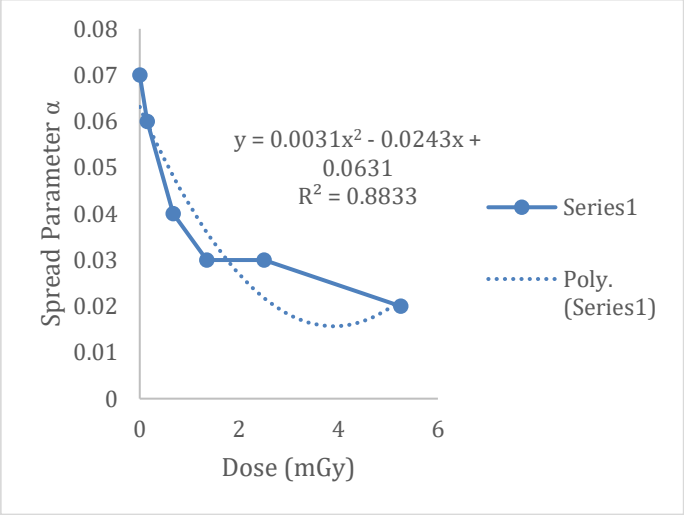
The mathematical models given below describe the effect of X-rays on the rat skin in terms of spread parameter, relaxation time and dielectric decrement;

Spread Parameter

Frequency range 20 Hz to 20 kHz

Rat skin: y = -9E-6x^2 + 0.0003x + 0.0703

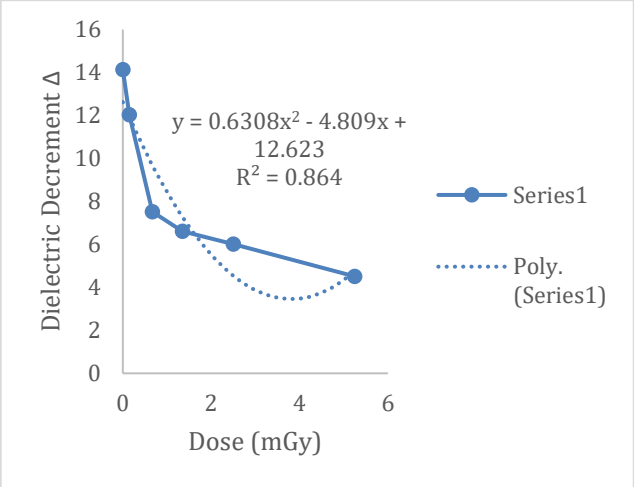
The quadratic terms quantify the relaxation of bound water, the effects of membrane capacitance and the structural heterogeneity (Foster, 2020), while the linear terms quantify ionic diffusion processes, counter-ion polarisation and interface phenomena (Castro et al., 2021).



Dielectric Decrement

Rat Skin at frequency range of 20 Hz to 20 kHz

y = -0.0015x2 + 0.0326x + 14.18



Relaxation Time

Rat Skin at frequency range of 20 Hz to 20 kHz

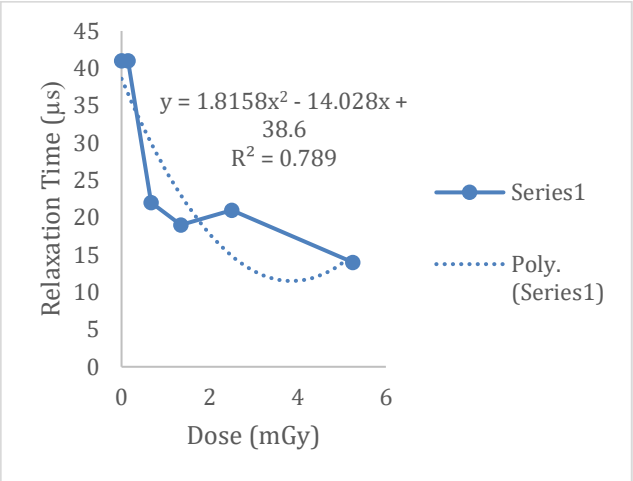
$y = -0.0053x2 + 0.2054x + 41.245$

All equations follow the general form:

$\alpha(f) = af^2 + bf + c$ (Sombo et al., 2015)

where f is the frequency (Hz), a is curvature coefficient, b is linear coefficient, and c is the baseline spread parameter.

The spread parameter, dielectric decrement, and relaxation time of X-irradiated rat skin follow a downward-opening parabolic trend, first increasing with frequency before reaching a peak and then declining within the 20 Hz to 20 kHz range, according to the negative quadratic coefficients ($a < 0$) in all three models



The regression charts shows that the dielectric decrement Δ of 0.86 and spread parameter α of 0.88 are good fits.

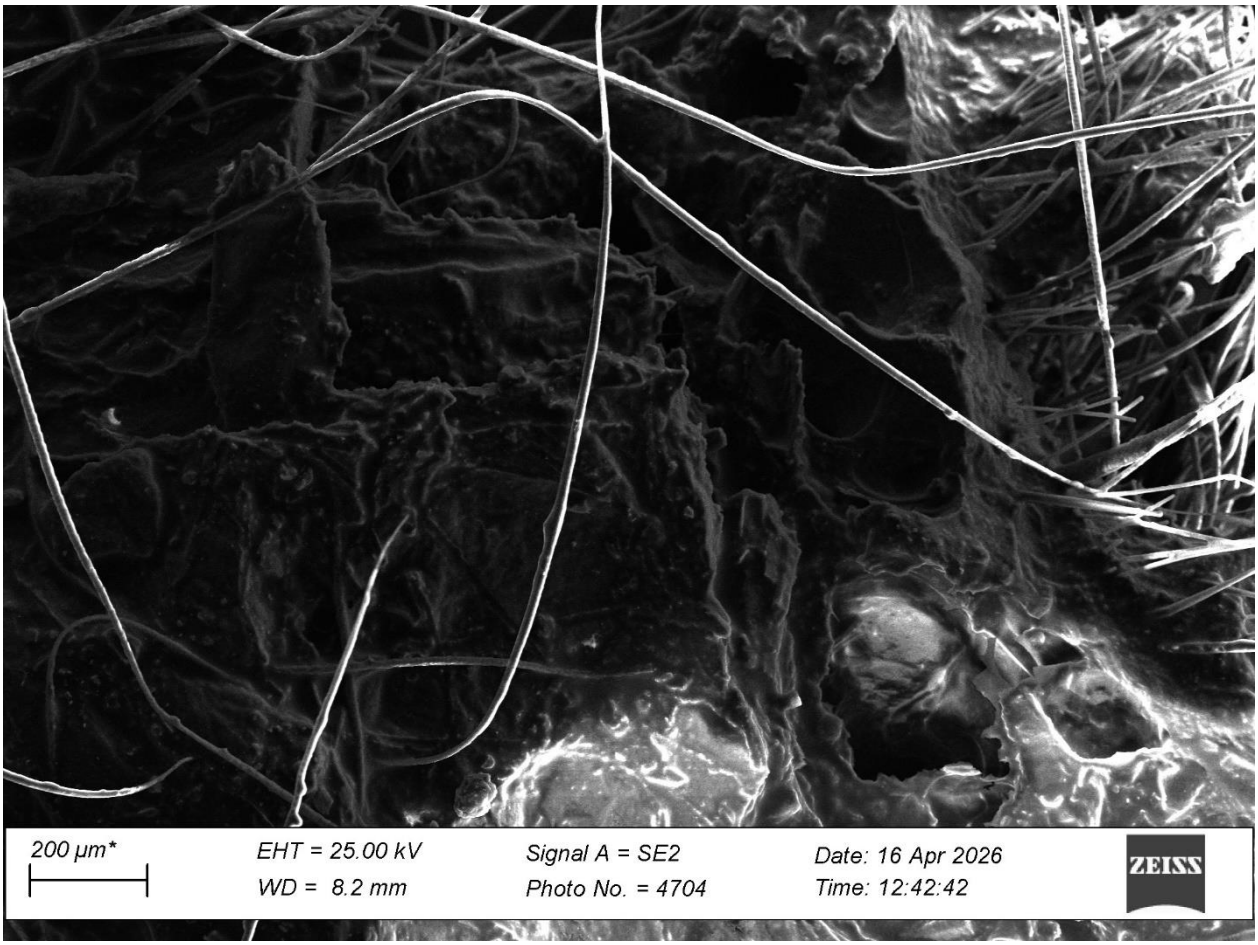


Figure 1: A SEM image of non-irradiated skin tissue of an albino rat.

Numerous long, thin, thread-like fibres are visible in the upper and right regions. These fibres are probably stray hair or collagen bundles from the skin. The fibres spread across deep holes and point in a variety of directions. There are black pits and big, deep holes in the centre-right region. The mass of tissue on the left is thicker and more textured. The skin layer is disorganized and fractured. In the upper-right corner, tiny fibres have bright white borders. The surface is extremely uneven and rough, with a three-dimensional shape, as seen by the deep black shadows and dazzling white patches.

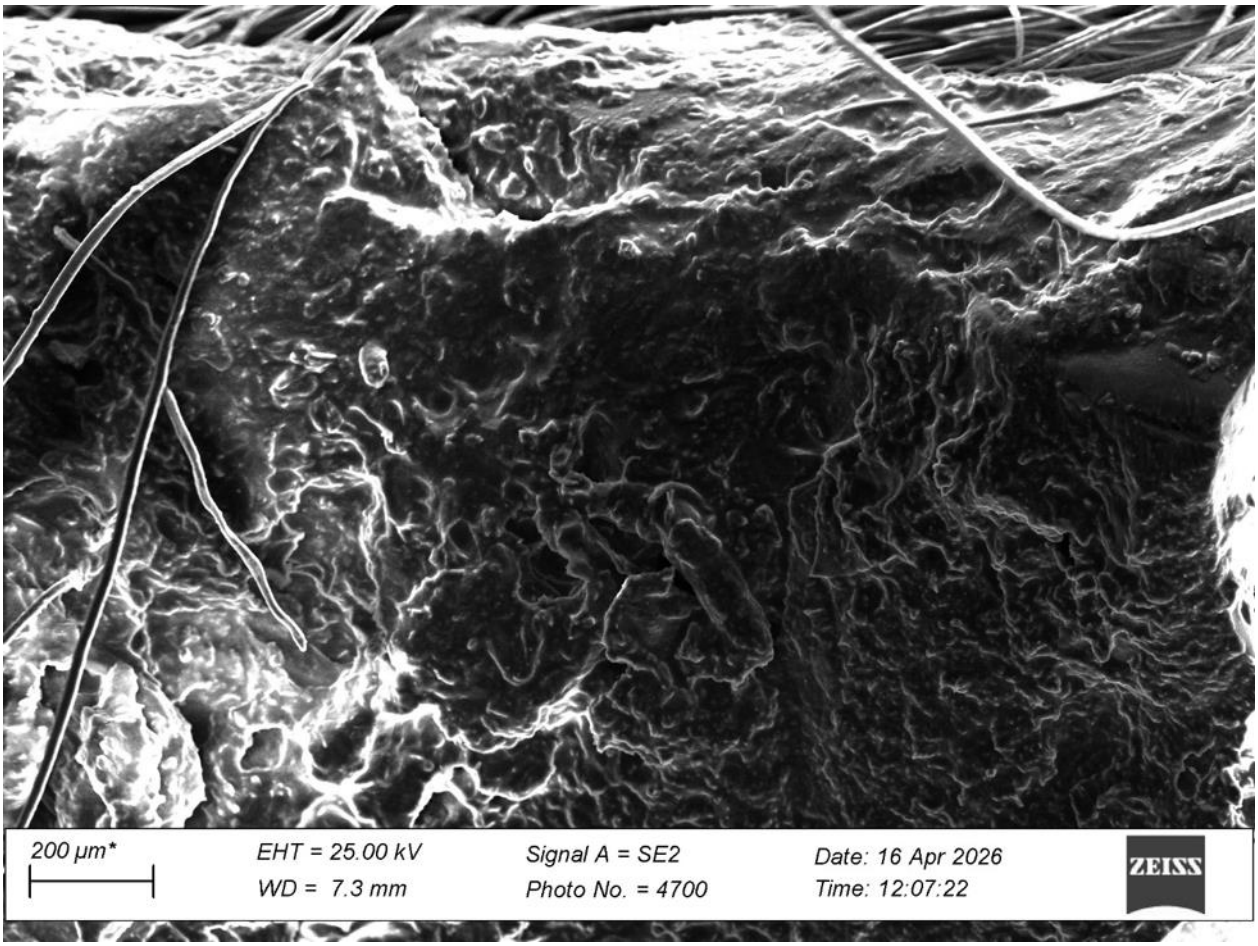


Figure 2: A SEM image of irradiated albino rats' skin tissue sample.

Figure 2 shows variations in surface compactness and fibre connectivity. There is a continuous tissue mass with wrinkles lower and center. The region has many small folds and wrinkles. The skin structure in this region is irregular and tightly packed.

There are signs of fibres splitting from the core tissue and breaking free at the outer margins. At the top edge and on the far left are long, thread-like fibres and hair-like strands that have separated from the bulk tissue. Above the deep and shadowy folds these loose strands shoot off at irregular angles across the top making discrete lines. The grey tones of the main tissue contrast sharply with the bright white margins of these projecting fibres, revealing an extremely uneven surface with a lot of small-scale roughness.

There is an obvious difference in the porosity, level of degradation and cohesiveness of the matrix of the two skin samples (figures 1 and 2). The control skin shows a loose open web of fibres with huge gaps larger in size, while the irradiated skin appears more compacted, wrinkled and compressed.

SEM comparison after low radiation dose of 5.25 mGy shows clear physical changes in the skin tissue. In the control skin, the majority of the open, dispersed network of fibres was composed of collagen and extracellular matrix (ECM) filaments with deep, empty spaces in between. This open, porous structure indicates the healthy, relaxed state of skin components at high vacuum.

The irradiated skin, in contrast, has a surface that is highly wrinkled, dense, continuous and compacted. Tissue under the radiation shows many small wrinkles and compressed folds as if it had contracted or compressed. The bulk of the tissue is still densely packed but at the upper margins a few loose fibres can be seen. This shows that the proteins and cells in the skin dehydrate from low doses of radiation and they shrivel up and wrinkle.

Simulation of X-Ray Absorption

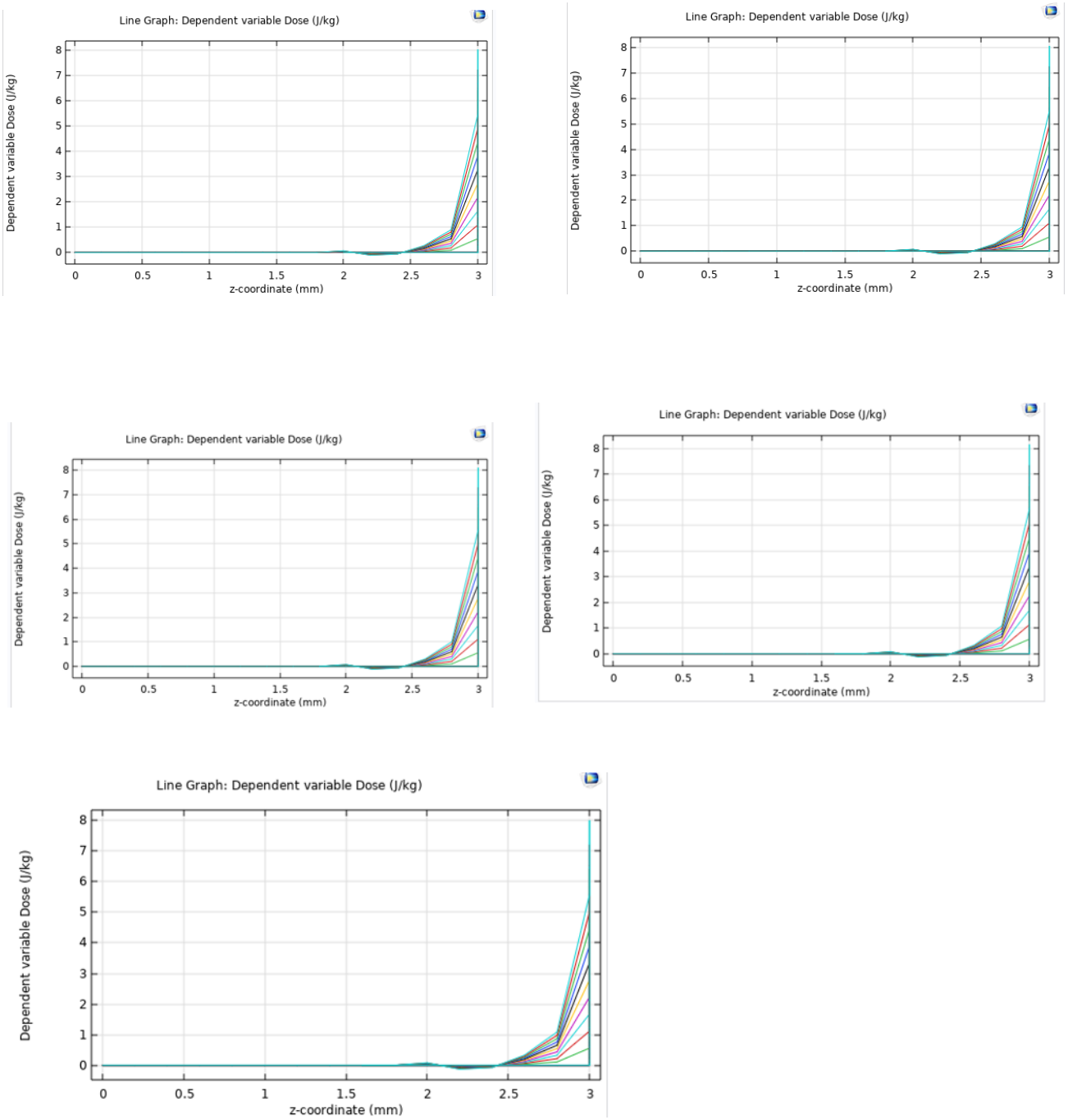


Figure 3: 1-D Plot graphs for skin tissues at varying dose showing the point of absorption and attenuation of X-rays

The 1-D plots of Figure 3 display that the x-axis is plotting depth in millimetres (0 to 3 mm). The x-ray beam comes from the right at z = 3 mm into the material boundary. From this it can be inferred that the radiation dose reaches an absolute maximum (between 4 and 8 J/kg) at the 3 mm mark.

X-rays interact with matter through processes such as Compton scattering and the photoelectric effect, losing energy and intensity while traversing (Feist & Plankensteiner, 2024). Another name for this is attenuation. The absorbed dose sharply decreases as soon as the x-rays enter the material and travel from right to left (from z = 3 mm down toward z = 2 mm). The dose decreases to 0 J/kg by the time the radiation reaches just 1 mm into the material (at z = 2 mm). For the rest of the tissue, the dose remains zero (from z = 2 mm to z = 0 mm).

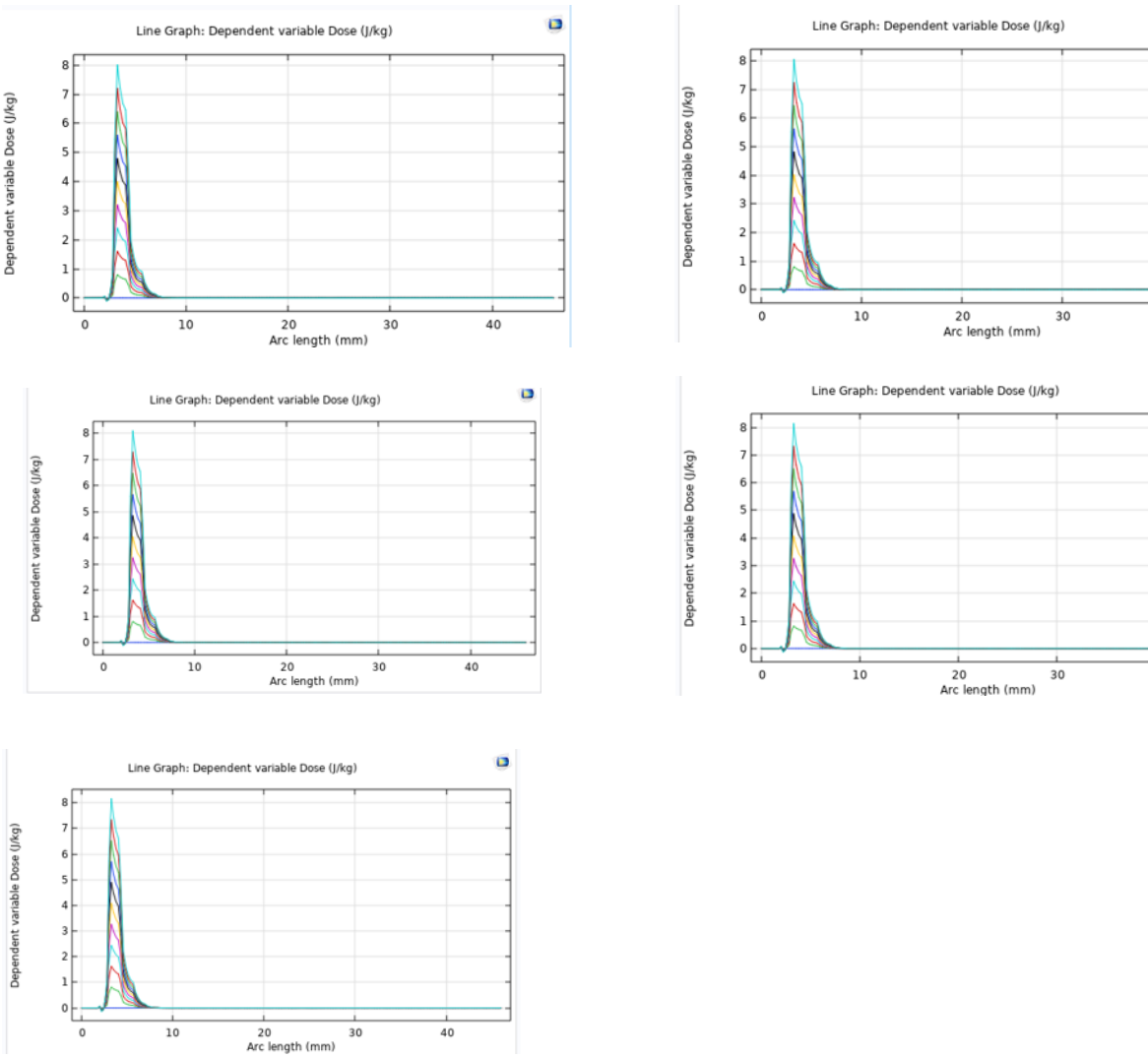


Figure 4: 1-D Plot graphs for skin tissues at varying dose showing the point of absorption and attenuation of X-rays (A=65, B=70, C=75, D=85, E=95 kVp)

The dependent variable dosage (J/kg) is the absorbed radiation dosage (1 J/kg = 1 Grey (Gy)) and is presented on the Y-axis of the charts in Figure 4 above. The arc length (mm) on the X-axis indicates the depth of penetration or path length into the medium. The graph shows a high peak near the entrance surface (around an arc length of 1 to 3 mm), which is followed by a fast, nearly exponential decrease that approaches zero as the path length increases above 10 mm.

The activity depicted in these graphs is very typical of x-rays travelling through matter, where photons strike the surface and start producing secondary electrons right away via Compton scattering and the photoelectric effect. This causes a quick build-up to a maximum dose relatively near the contact (around 2 mm in this case). Additionally, x-rays interact probabilistically during their whole course since they are uncharged particles. The Beer-Lambert Law states that once they attain peak ionization, their intensity decreases exponentially ($I \alpha e^{-\mu x}$).

As the arc length increases from 3 mm to more than 10 mm, this explains the lengthy, smooth downhill slope. X-rays have a theoretically unlimited range and a continuous attenuation profile. Until the beam is totally attenuated, they keep depositing dose throughout the material (Berman et al., 2015).

CONCLUSION

The macroscopically observed dielectric behaviour of mouse cutaneous tissues was satisfactorily correlated with low-dose ionizing radiation in this investigation. A highly cohesive multi-scale bio-electromagnetic analytical framework was created by combining structural Cole-Cole modelling, high-resolution SEM microstructural evaluation, computational COMSOL Multiphysics X-ray propagation simulations, and low-frequency dielectric spectroscopy (20 Hz to 20 kHz).

The empirical results show that exposure to X-ray radiation within a small 0.15 to 5.25 mGy window causes a severe, monotonic collapse of its core capacitive parameters, whereas non-irradiated cutaneous tissue retains classic α- and β-dispersion kinetics controlled by Maxwell-Wagner interfacial polarization. The skin showed a significant 68% reduction in static permittivity (εs decreasing from 22.84 to 7.29) and a comparable decrease in total dielectric strength (Δε) at the maximal exposure threshold of 5.25 mGy. Radiation-induced structural protein denaturation and a systemic decrease in the volume of orientable dipoles inside the unravelling tissue matrix are the direct causes of this sweeping reduction, which emphasizes a significant decline in overall polarization capability. At the same time, the characteristic relaxation period (τ) dropped dramatically from 41 μs to 14 μs. The phenomena of macromolecular fragmentation—the systematic disintegration of larger, slow-moving cellular borders into smaller, highly porous, and more quickly reorienting dipolar units—is validated by this kinetic acceleration.

High-resolution SEM micrographs, which show a structural change from a tightly bonded, cohesive dermal matrix in control specimens to a broken, extensively separated, and porous state post-irradiation, visibly and physically support these electrical trends. Additionally, the physical energy transport mechanics were successfully mapped by the 2D axisymmetric COMSOL model, which localized peak X-ray energy attenuation close to a crucial focal depth barrier of 3 mm when spatial absorbed dose configurations reached about 8 J/kg.

In summary, this work thoroughly demonstrates that structural membrane integrity is directly compromised and dipole relaxation kinetics are altered by low dose ionizing radiation, which modifies macroscopic soft tissue electrical activity. For contemporary radiobiology, the exact tissue-specific relaxation constants, dispersion coefficients, and mathematical regressions obtained here offer useful baseline parameters. In the end, these discoveries close the historical gap between macro scale bio impedance measurements and microscopic radiochemical degradation, providing a solid technical basis for the creation of non-invasive, real-time bio impedance diagnostic sensors for early-stage radiation damage assessment.

Conflict of Interest Statement

The authors declare that the research was conducted in the absence of any commercial or financial relationships that could be construed as a potential conflict of interest.

References

Agba, E.H., Laogun, A.A., & Ajai, N.O. (2008). A comparison of the effect of diagnostic x-rays on the radiofrequency dielectric properties of bovine liver with bovine kidney tissues. Nigerian Journal of Physics, 20 (1), 11-22

Aberg P, Geladi P, Nicander I, Hansson J, Homgren U & Ollmar S. (2005) Non-invasive and microinvasive electrical impedance spectra of skin cancer- a comparison between two techniques. Skin Res. Technol. II, 281-286.

Berman, A.T., St. James, S., Rengan, R. (2015). Proton beam therapy for non-small cell lung cancer: current clinical evidence and future directions. Cancers,7, 1178-90; doi: 10.3390/cancers7030831

Castro, R., Spivak, Y., Shevchenko, S., & Moshnikov, V. (2021). Low-Frequency Dielectric Relaxation in Structures Based on Macroporous Silicon with Meso-Macroporous Skin-Layer. Materials, 14(10), 2471. https://doi.org/10.3390/ma 14102471

Ferreira D.M., Silva C.S., & Souza M.N. (2007). Electrical Impedance model for evaluation of skin irritation in rabbits and humans. Skin Res. Technol. 13 259-267.

Feist, C., & Plankensteiner, A. (2024) Monte-Carlo model for radiation transport in solid x-ray targets. COMSOL Conference. 1-7.

Foster, K.R. (2008). Dielectric properties of biomaterials & biomedical engineering. 2nd Edition, CRC Press. 11. ISBN 9780429154065.

Gabriel, S., Lau, R. W., & Gabriel, C. (1996). The dielectric properties of biological tissues: III. Parametric models for the dielectric spectrum of tissues. Physics in Medicine & Biology, 41(11), 2271–2293.

Gabriel, S., Lau, R. W., & Gabriel, C. (1996). The dielectric properties of biological tissues: II. Measurements in the frequency range 10 Hz to 20 GHz. Physics in medicine and biology, 41(11), 2251–2269. https://doi.org/10.1088/0031-9155/41/11/002.

Huclova S., Erni D., Frohlich J. (2012). Modelling and validation of dielectric properties of human skin in the MHz region focusing on skin layer morphology and material composition. J. Phys. D: Appl. Phys. 45 doi:10.1088/0022-3727/45/2/025301.

Iyomasa M.M., Leao J.C., Rizzi E.C., Issa J.P.M., Dias F.J., Watanabe I., Iyomasa D.M., (2014). Ultrastructure and light microscope analysis of intact skin after a varying number of low level laser irradiation in mice. Biomed. Research International. http://dx.doi.org/10.11552014/506051.

Jonscher, A. K. (1999). Dielectric relaxation in solids. Journal of Physics D: Applied Physics, 32(14), R57–R70. https://doi.org/10.1088/0022-3727/32/14/201

Kremer, F., & Schönhals, A. (Eds.). (2003). Broadband dielectric spectroscopy. Springer-Verlag. https://doi.org/10.1007/978-3-642-56120-7

Marzec E. & Warchol W. (2005). Dielectric properties of a protein water system in selected animal tissues. Bioelectrochemistry 65 89-94

Orkaa, M. S., Bello, A. A., Dlama, J. Z., Ewuga, U. J. (2024) Evaluating the Dielectric Characteristics of Tissues: A Relationship Between Low Frequency Range and Dryness. Nigerian Journal of Physics 33(2): 146-156.

Pethig, R. (2018). Dielectric and electrical properties of biological materials. Electromagnetic Biology and Medicine 4(2):7-9 DOI: 10.3109/15368378509033258

Peyman, A., Rezazadeh, A. A., & Gabriel, C. (2015). Changes in the dielectric properties of rat tissue as a function of age at microwave frequencies. Physics in medicine and biology, 46(6), 1617–1629. https://doi.org/10.1088/0031-9155/46/6/303

Sombo, T., Ige, T. A., & Agba, E. H. (2015). Mathematical Modelling of the Effects of Gamma Irradiation on Dielectric Dispersion of Bovine Liver Tissues at Low and Radiofrequency. 5(1), 12–17. https://doi.org/10.5923/j.biophysics.20150501.02

Walker D C., Brown B.H., Smallwood R.H., Hose D.R., & Jones D.M. (2002). Modelled current distribution in cervical squamous tissue. Physiol. Meas. 23 159-168.

Zimmermann J, & van Rienen U. (2021). Ambiguity in the interpretation of the low frequency dielectric properties of biological tissues. Bioelectrochemistry 140.

Appendix

REF: FUL/DIRECT/ECC/2026/HU:0008

Office of the Vice Chancellor

Directorate of Research & Creative Thoughts

RESEARCH ETHICAL CLEARANCE CERTIFICATE

This is to certify that the Study titled..MEASUREMENT AND MODELLING OF DIELECTRIC PROPERTIES OF SELECTED X-IRRADIATED AND NON-IRRADIATED TISSUES OF ALBINO RATS.....

to be carried out at...FEDERAL UNIVERSITY OF LAFIA.....

from this Day .../11... Month..July.....2026..has been granted ethical clearance approval

Name of Researcher/ Principal Researcher...MIIONGO STEPHEN ORKAA.....

29th July, 2026

Director, Research & Creative Thoughts